

## A Laterally Modulated 2D Electron System in the Extreme Quantum Limit

S. Melinte,<sup>1</sup> Mona Berciu,<sup>2</sup> Chenggang Zhou,<sup>1</sup> E. Tutuc,<sup>1</sup> S. J. Papadakis,<sup>1</sup> C. Harrison,<sup>3</sup> E. P. De Poortere,<sup>1</sup> Mingshaw Wu,<sup>3</sup> P. M. Chaikin,<sup>3</sup> M. Shayegan,<sup>1</sup> R. N. Bhatt,<sup>1</sup> and R. A. Register<sup>4</sup><sup>1</sup>Department of Electrical Engineering, Princeton University, Princeton N.J. 08544<sup>2</sup>Department of Physics and Astronomy, University of British Columbia, Vancouver B.C. V6T 1Z1, Canada<sup>3</sup>Department of Physics, Princeton University, Princeton N.J. 08544<sup>4</sup>Department of Chemical Engineering, Princeton University, Princeton N.J. 08544

(Dated: April 14, 2024)

We report on magnetotransport of a two-dimensional electron system (2DES), located 32 nm below the surface, with a surface superlattice gate structure of periodicity 39 nm imposing a periodic modulation of its potential. For low Landau level fillings, the diagonal resistivity displays a rich pattern of oscillations, even though the disorder dominates over the periodic modulation. Theoretical arguments based on the combined effects of the long-wavelength, strong disorder and the short-wavelength, weak periodic modulation present in the 2DES qualitatively explain the data.

PACS numbers: 73.40.Rw, 73.43.Fj, 71.70.Df

Two-dimensional electron systems (2DESs) subjected to both an artificial periodic modulation and a quantizing, perpendicular magnetic field  $B$  are expected to exhibit remarkable behavior arising from the interplay of the period of the modulation and the magnetic length, and the relative strengths of the periodic modulation, cyclotron energy ( $\hbar\omega_c$ ), and disorder potential [1, 2, 3]. When the periodic modulation's strength is weak compared to  $\hbar\omega_c$ , each of the highly degenerate Landau levels (LLs) evolve into an energy spectrum with recursive properties, the so-called Hofstadter butterfly. In this limit, the structure of the butterfly is controlled by the ratio of the magnetic flux through the unit cell area  $A$  of the periodic modulation,  $\Phi = BA$ , to the flux quantum  $\Phi_0 = h/e$ . Optimally,  $\Phi = \Phi_0$  should be of order unity and  $B$  should be large so that well-separated LLs are formed. This poses the stringent requirement of a small unit cell area  $A$ . Additionally, the disorder, present in any real system, should be small compared to the strength of the periodic potential, so that the butterfly's larger energy gaps remain open. Then, one may probe directly the effects of the periodic modulation within a single, resolved LL. In particular, maxima and minima are expected in the low-temperature ( $T$ ) diagonal resistivity  $\rho_{xx}$  as  $B$  is swept at fixed density  $n$  through a LL, i.e. as the Fermi level ( $E_F$ ) moves through the subbands and subgaps of the butterfly. Yet, for realistic disorder-broadened LLs, new physics can occur, due to the competition between the strengths of the disorder and the periodic modulation.

Here we present low- $T$  magnetotransport measurements in a GaAs/AlGaAs 2DES, at a distance of 32 nm below the surface, whose potential is modulated via a surface gate with triangular symmetry and a periodicity of 39 nm, the smallest periodicity yet reported [4, 5, 6]. Moreover, our data are taken in the extreme quantum limit, i.e. at low LL fillings where the integer quantum Hall effect [7] is observed. Despite the high quality of the

2DES and its close proximity to the modulating gate [8], the disorder induced by doping impurities, located at a distance of 20 nm, is much larger than the periodic potential. Naively, one may expect that in this regime where the periodic potential is only a small perturbation, it should play no significant role in the transport properties of the system. Surprisingly, our results reveal that the small periodic potential does play a large role. Experimentally, we observe that the lowest spin-down LL is significantly broadened and  $\rho_{xx}$  at low  $\nu$  exhibits a rich oscillation pattern. Our theoretical arguments, based on the combined effects of the weak, short-wavelength periodic potential and the strong, long-wavelength disorder, qualitatively explain the data. The results highlight the importance of the very different length scales of the disorder and the periodic potentials in determining transport through the 2DES: because there are large areas of the sample where the disorder potential is very flat, the periodic potential plays the dominant role locally (this is one of the rare cases in physics where a small perturbation has a significant and non-trivial effect).

The sample studied here was grown by molecular beam epitaxy, and consists of a GaAs/Al<sub>0.3</sub>Ga<sub>0.7</sub>As heterostructure with a 2DES ( $n \approx 3 \times 10^{11} \text{ cm}^{-2}$ ) at a distance  $d = 32 \text{ nm}$  below the surface. The Si dopant atoms were deposited at a distance of about 12 nm below the surface. The low- $T$  mobility, prior to and after the patterning, is about  $3 \times 10^5 \text{ cm}^2/\text{Vs}$ . Experiments were performed on 20  $\mu\text{m}$ -wide Hall bars fabricated by standard photolithography and wet etching. The distance between the probes used to measure the resistivity was 20  $\mu\text{m}$ . The resistivity coefficients [9] were measured by probe pairs located in different regions of the Hall bar, yielding qualitatively similar results. The 2DES is placed in a periodic potential created by a top gate realized by means of a diblock copolymer nanolithography technique [10]. First, a self-assembled layer of hexagonally-ordered polyisoprene nano-domains (spheres with center-

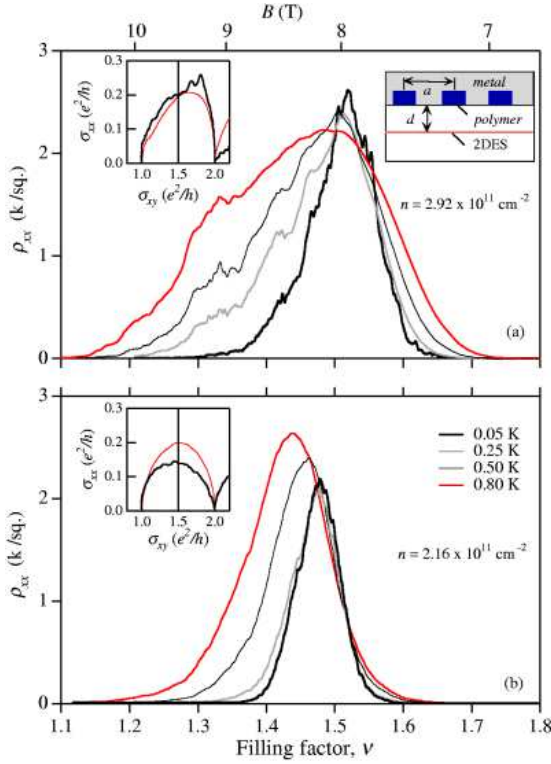


FIG. 1: (color online)  $\rho_{xx}$  vs  $\nu$  traces for (a) the patterned sample at  $V_g = 0$  V and (b) unpatterned sample at indicated temperatures. The top magnetic field scale is for the data of panel (a). Left insets:  $\sigma_{xx}$  vs  $\sigma_{xy}$  at  $T = 0.05$  and  $0.80$  K. Right inset: side-view of the device.

to-center distance  $a$ ) contained in a polystyrene matrix was formed on the sample's surface. After the removal of the polyisoprene spheres a polystyrene mask  $15$  nm-thick is left on the surface and acts as a template for a Ti/Au metallic gate, whose potential  $V_g$  can be varied [see right inset to Fig. 1 (a)]. Even without applying an external gate bias, a rich structure is present in the  $\rho_{xx}$  data for the patterned sample. This observation corroborates with the results of previous experiments [5, 6] and theoretical calculations [11] which explain the modulation at zero bias through the effects of strain and Fermi level pinning at the semiconductor-metal (gate) interface.

The central result of our experimental work is shown in Fig. 1 where  $\rho_{xx}$  is displayed in the filling factor range  $1.1 < \nu < 1.8$  at various temperatures for the patterned and unpatterned samples [9]. Several features of the data are noteworthy. (1) For both samples,  $\rho_{xx}$  exhibits a maximum centered around  $\nu = 3/2$  and shows reproducible oscillations at low  $T$  [12]. For the modulated sample, however, the observed oscillations in  $\rho_{xx}$  are much stronger. Qualitatively similar data was reported in Ref. 4 for a similar device with  $60$  nm periodicity, giving further evidence that these oscillations are intrinsic. (2) Compared to the data taken in the unpatterned sample,  $\rho_{xx}$  is dramatically distorted in the patterned sam-

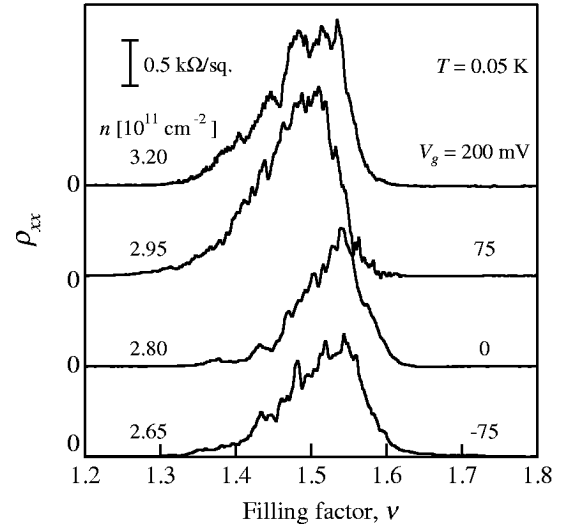


FIG. 2:  $\rho_{xx}$  vs  $\nu$  at  $T = 0.05$  K and various  $V_g$  ( $n$ ). Curves for  $V_g = 0, 75$ , and  $200$  mV have been shifted for clarity.

ple and has an extended tail on the low- $\nu$  side. To better illustrate the observed asymmetry for the patterned sample, we display in the insets to Fig. 1 the  $\rho_{xx}$ ,  $\rho_{xy}$  flow diagram [7, 9]. We note that both the  $\rho_{xx}$  oscillations and the asymmetry are reproducible with repeating B-sweeps and also varying  $T$  in the low temperature range. (3) As  $T$  is raised, concomitantly with the weakening of the  $\nu = 1$  QHE minimum, new peaks develop, growing out from the  $\rho_{xx} = 0$  background. The peak near  $\nu = 3/2$  broadens with increasing temperature and displays at  $T = 0.80$  K a full-width at half-maximum (FWHM) up to four times larger than the low- $T$ , saturated FWHM. In contrast, the FWHM in the unpatterned sample increases only by a factor of two for the same  $T$  range. (4) As seen in Fig. 2, where we present our lowest temperature  $\rho_{xx}$  as a function of  $\nu$  for various gate voltages, the oscillations appear predominantly on the low- $\nu$  side of the peak, regardless of the sign of  $V_g$ .

We now discuss the properties of the Hofstadter spectrum for parameters relevant to our sample. In the absence of disorder, and neglecting LL mixing, the electronic structure is a function only of the ratio  $\phi = \phi_0$ . For  $\phi = \phi_0 = q/p$ , with  $p$  and  $q$  mutually prime integers, the Landau band splits into  $q$  subbands. The Hofstadter butterfly for a repulsive  $V_1 > 0$  weak triangular modulation  $V(x; y) = 2V_1 \cos \frac{2\pi}{a^2/3} (x + \frac{1}{3}y) + \cos \frac{2\pi}{a^2/3} (x - \frac{1}{3}y) + \cos \frac{4\pi}{a^2/3} x$  is shown in Fig. 3. The energies of the eigenstates are referenced to the lowest LL energy  $\hbar\omega_c/2$  and are scaled by the amplitude of the first Fourier component of the periodic potential  $V_1$  [2]. While the number of total subbands  $q$  jumps discontinuously as  $B$  is varied, from Fig. 3 it is apparent that for all  $\phi = \phi_0/2 (m; m+1)$ , where  $m$  is an integer, the butterfly has precisely  $m+1$  main subbands, each of which

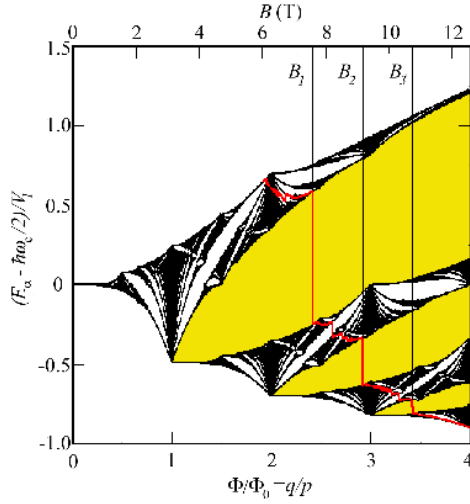


FIG. 3: (color) Hofstadter butterfly of the spin-down lowest LL for a weak, repulsive, triangular potential modulation. The eigenenergies are plotted vs  $q/p$ , for  $p$  and  $q$  between 1 and 150. The position of  $E_F$  is shown by the red curve.

has a fractal structure of its own. Simple arguments show that the total number of states per unit area in each of the upper main subbands is  $n_0 = 1/A$ , whereas the lowest main subband contains the rest of  $[(m_0) - 1]n_0$  states of the LL [13]. The three subgaps shown as yellow regions in Fig. 3 are the most robust against disorder: if disorder is small, one expects to see minima in  $\sigma_{xx}$  when  $E_F$  is inside these subgaps ( $\sigma_{xx}/\sigma_{xx}^0$ , [9]). For a given  $n$  we find the magnetic field  $B_i$  at which  $E_F$  is inside each of the main subgaps of the spin-down lowest LL to be  $B_i = \phi_0/2(n + m_0)$ . For  $n = 2.92 \times 10^{11} \text{ cm}^{-2}$  ( $V_g = 0$  in Fig. 1),  $E_F$  should cross the main subgaps at  $B_1 = 7.6 \text{ T}$ ,  $B_2 = 9.2 \text{ T}$ , and  $B_3 = 10.7 \text{ T}$  ( $\phi_0 = 1.59, 1.31, \text{ and } 1.13$ ). Figs. 1 and 2 show that the low- $T$   $\sigma_{xx}$  vanishes for all  $\phi_0 < 1.3$  and  $\phi_0 > 1.6$ , suggesting that all states, except for a few in the second highest subband, are fully localized. The same conclusion is reached if the analysis is repeated for an attractive potential  $V_1 < 0$ , for which the Hofstadter structure of Fig. 3 is inverted.

These observations indicate that disorder plays an important role. From the measured low- $T$  mobility we estimate the width of the disorder-broadened LLs at  $0.24 (\text{B [T]})^{1/2} \text{ meV}$  [3]. For  $B = 10 \text{ T}$  it is  $0.7 \text{ meV}$ , much larger than  $V_1 = 0.1 \text{ meV} = V - V_g$  ( $V$ ) inferred from the exponentially decaying solution of the Laplace equation [8]. Although the modulation amplitude is not precisely known [11], in our sample it likely remains smaller than the disorder. Since the main subgaps are filled in by disorder, the features in  $\sigma_{xx}$  ( $\sigma_{xx}$ ) cannot be attributed to  $E_F$  crossing the smaller gaps inside the second subband (from  $B_1$  to  $B_2$ ); these smaller gaps must also be filled in by disorder. Hence, an interpretation of our data based on the naive Hofstadter butterfly is inappropriate.

In order to understand the origin of the  $\sigma_{xx}$  features,

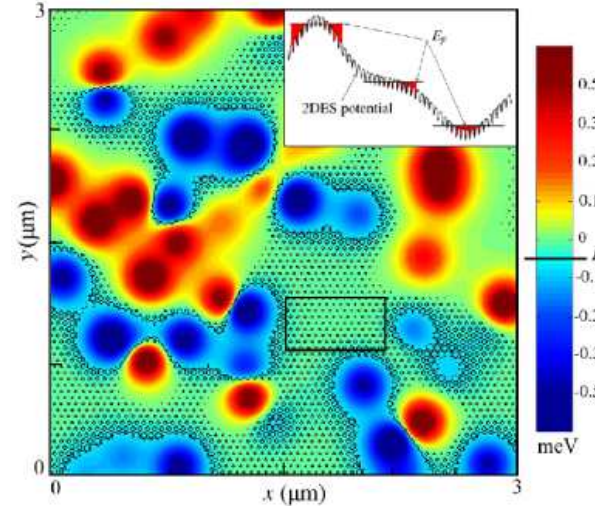


FIG. 4: (color) The equipotential contours (black curves) of the total 2D ES potential at  $\phi_0 = 1.3$ . The 2D ES potential consists of a weak, attractive, triangular periodic modulation and a slowly varying disorder potential. Minima (maxima) of the disorder potential are shown in blue (red). The inset schematically shows  $E_F$  crossing through the 2D ES potential.

we must analyze the new regime of a small periodic modulation and large disorder. Slowly-varying disorder (expected in high-mobility, remotely-doped samples such as ours) can be treated in semiclassical terms, with wavefunctions following the equipotentials of the disorder. The LLs are broadened, with all high (low) energy states being localized near maxima (minima) of the disorder potential. Current-carrying extended states correspond to equipotential contours percolated across the sample and are found in a so-called critical region at the center of the Landau band [7]. The effect of a supplementary weak periodic potential is illustrated in Fig. 4, where we plot equipotential contours of the total 2DES potential. The disorder potential is a sum of screened Coulomb potentials from doping impurities located 20 nm from the 2DES [14]. The amplitude of both disorder and the periodic potentials are close to experimental estimations. Instead of smooth trajectories, the equipotential contours now have a fractured nature, with many little "bubbles" around minima of the periodic potential located at areas of the disorder potential. Since the lattice constant  $a$  is comparable to the magnetic length, quantum mechanical tunneling spreads the electronic wave-functions over these flat regions, and considerably helps their percolation throughout the sample. This picture is in qualitative agreement with the results of Figs. 1 and 2, which show that  $\sigma_{xx}$  of the patterned sample is considerably enhanced with increasing  $T$  on the low- $T$  side, suggesting transport through temperature-activated hopping between nearby states, absent in the unpatterned sample.

This picture also offers a possible explanation for the detailed peak and valley structure observed in our magne-

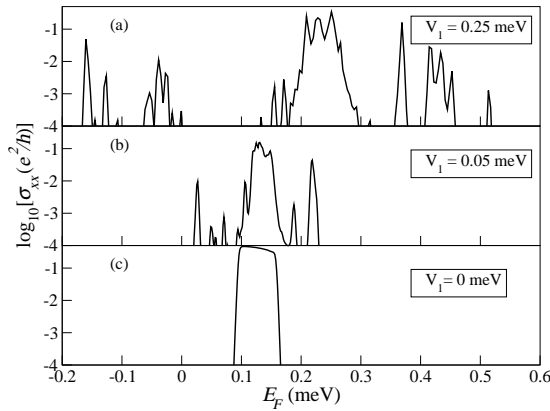


FIG. 5:  $\sigma_{xx}$  vs  $E_F$  for a  $31 \times 29 \text{ nm}^2$  sample at  $T = 0.01 \text{ K}$  and indicated  $V_1$  for  $q=p=5=2$ . The standard deviation of the disorder potential is  $0.7 \text{ meV}$ .  $E_F$  is measured from  $\hbar\epsilon_c=2$ .

to transport data. Consider the area enclosed in the rectangle drawn in Fig. 4, which is almost disorder-free (it has very little underlying disorder variation). Wave-functions across such flat regions correspond to those of finite-area Hofstadter butterflies, with appropriate boundary conditions. For the appropriate energy range,  $E_F$  is either inside a subband or a gap of such local Hofstadter structures. If  $E_F$  is inside a subband, wave-functions span the flat region and help enhance the percolation. When  $E_F$  is inside a gap, there are no states supported by the flat region and hence, no current can flow across it. Such flat regions act as switches which are turned on or off as  $E_F$  is changed, helping or hindering the current flow through the sample. When one or more switches are off, there are fewer paths for the current to be carried across the sample, and a valley is expected in  $\sigma_{xx}$  ( $\sigma_{yy}$ ).

Finally, the appearance of the fluctuation pattern preponderantly on the low- $\sigma$  side (see Fig. 2) is a direct consequence of the particle-hole asymmetry of the triangular potential. For LL filling factors  $1 < \nu < 3=2$  ( $3=2 < \nu < 2$ ), percolation between wave-functions localized around minima (maxima) of the disorder is helped by the "bubbles" centered on them (minima) of the periodic potential (see inset to Fig. 4). When attractive, the triangular potential has deep minima on a triangular pattern, and shallow maxima on a displaced honey-comb pattern (notice that there are almost no honey-comb arranged "bubbles" in Fig. 4). For  $3=2 < \nu < 2$ , the shallow maxima of the periodic potential are not as effective in enhancing percolation, and  $\sigma_{xx}$  ( $\sigma_{yy}$ ) in the modulated sample is similar to that of the unpatterned sample.

These semiclassical arguments are supported by preliminary computations of  $\sigma_{xx}$ , shown in Fig. 5, based on the Kubo-Landauer formalism [14]. The calculation is done for a given realization of a slowly-varying disorder potential and for a fixed value of  $B$ . As  $\nu$  is varied from  $2.6$  to  $3.4 \times 10^{11} \text{ cm}^{-2}$ ,  $E_F$  sweeps through the disorder broadened LL. In Fig. 5(a), the peak-to-peak amplitude

of the periodic modulation  $\sim 9V_1$  for the triangular superlattice is somewhat larger than disorder's strength. Well-defined subbands start to separate and evolve towards the Hofstadter butterfly structure expected in the limit where disorder becomes negligible compared to the periodic modulation. In the opposite limit of no periodic modulation [Fig. 5(c)], we observe a narrow, smooth peak when  $E_F$  is inside the critical region of percolated states (not centered at  $E = 0$  because the disorder potential is not particle-hole symmetric). For a periodic modulation weaker or comparable to the disorder strength [Fig. 5(b)], a pattern of peaks and valleys emerges, as the periodic potential influences the percolation inside and near the critical region. Efforts to improve the description of the disorder potential are under way, so that quantitative comparisons with the experiment become possible.

To conclude, our work extends the rich problem of modulated 2DESs in quantizing magnetic fields to a new regime of long-wavelength, strong disorder and short-wavelength, weak periodic potential, and uncovers yet more interesting physics.

This work is supported by a NSF/NATO Grant, a NSF MRSEC Grant and by NSERC of Canada (M.B.).

---

corresponding author: berciu@physics.ubc.ca

- [1] D.R. Hofstadter, Phys. Rev. B 14, 2239 (1976).
- [2] F.H. Claar and G.H. Wannier, Phys. Rev. B 19, 6068 (1979).
- [3] D. Pönnkuche and R.R. Gerhardt, Phys. Rev. B 46, 12606 (1992).
- [4] C.G. Smith et al., J. Vac. Sci. Technol. B 10, 2904 (1992).
- [5] T. Schlösser et al., Europhys. Lett. 33, 683 (1996).
- [6] C.A. Balbrecht et al., Phys. Rev. Lett. 86, 147 (2001).
- [7] The Quantum Hall Effect, edited by R.E. Prange and S.M. Girvin, (Springer-Verlag, New York, 1987).
- [8] The potential modulation seen by the 2DES is equal to the modulation of the periodic gate potential, attenuated by the factor  $\exp(-4\pi d/3a)$ . A low attenuation requires a large  $a/d$  ratio, which highlights the critical role of high quality shallow 2DESs for the experiments.
- [9] The longitudinal and transverse resistivities  $\sigma_{xx}$  and  $\sigma_{xy}$  were recorded at both positive and negative  $B$  to eliminate the mixing between transport tensor components.  $\sigma_{xx}$  and  $\sigma_{xy}$  were then determined from the standard relations  $\sigma_{xx} = (\sigma_{xx}^+ + \sigma_{xx}^-)/2$ ;  $\sigma_{xy} = (\sigma_{xy}^+ - \sigma_{xy}^-)/2$ .
- [10] C.H. Harrison et al., J. Vac. Sci. Technol. B 16, 544 (1998).
- [11] J.H. Davies and I.A. Larkin, Phys. Rev. B 49, 4800 (1994).
- [12] Several studies on narrow, quasi one-dimensional channels have revealed the presence of fluctuations in transport coefficients, predominantly near the breakdown of the QHE [J.A. Simmons et al., Phys. Rev. Lett. 63, 1731 (1989)]. The conduction mechanism in these narrow samples is consistent with the model of tunneling-assisted percolation between opposite edge states [J.K. Jain and S.A. Kivelson, Phys. Rev. Lett. 60, 1542 (1988)].
- [13] These values lead to the correct Chern numbers.

[14] C . Zhou, M . Berciu and R N . Bhatt (unpublished).